# New physical concepts for cell amoeboid motion

Evan Evans
Departments of Pathology and Physics, University of British Columbia, Vancouver, British Columbia, Canada V6T 1W5

ABSTRACT Amoeboid motion of cells is an essential mechanism in the function of many biological organisms (e.g., the regiment of scavenger cells in the immune defense system of animals). This process involves rapid chemical polymerization (with numerous protein constituents) to create a musclelike contractile network that advances the cell over the surface. Significant progress has been made in the biology and biochemistry of motile cells, but the physical dynamics of cell spreading and contraction are not well understood. The reason is that general approaches are formulated from complex mass, momentum, and chemical reaction equations for multiphase–multicomponent flow with the nontrivial difficulty of moving boundaries. However, there are strong clues to the dynamics that allow bold steps to be taken in simplifying the physics of motion. First, amoeboid cells often exhibit exceptional kinematics, i.e., steady advance and retraction of local fixed-shape patterns. Second, recent evidence has shown that cell projections "grow" by polymerization along the advancing boundary of the cell. Together, these characteristics represent a local growth process pinned to the interfacial contour of a contractile network. As such, the moving boundary becomes tractable, but subtle features of the motion lead to specific requirements for the chemical nature of the boundary polymerization process. To demonstrate these features, simple examples for limiting conditions of substrate interaction (i.e., "strong" and "weak" adhesion) are compared with data from experimental studies of yeast particle engulfment by blood granulocytes and actin network dynamics in fishscale keratocytes.

## INTRODUCTION

Amoeboid cells are essential components in an animal's defense against invading organisms. These cells (e.g., granulocytes, monocytes, macrophages, and so on) carry out their function in adverse physical environments like the high flow rate circulation. Attachment to vascular surfaces and movement into adjacent tissues require strong adhesivity and rapid motility. The exceptional deformability of these cells is made possible by the large excess of plasma membrane present in folds and other forms of surface roughness. Since the plasma membrane bilayer is fluid, it easily flows in response to extensional deformation within the constraint of total envelope area. In turn, the membrane is anchored to and shaped by the subsurface cortex of actin filaments that form a dynamic network (1–5). It is the chemical assembly, contraction, and disassembly of this network that drives cell motion.

Surprisingly, many features of amoeboid motion (even magnitudes of the speed of movement) cross species and/or cell type boundaries and thus appear to be universal principles for biological design in nature. Although general physical models have been formulated to represent amoeboid behavior (6–10), these scholarly approaches have failed to capture the kinematic simplicity often observed in cell spreading, i.e., steady phases of advance for local segments of the lamella with nearly fixed-shaped patterns. (When cells experience ubiquitous-environmental stimuli [e.g., leukocytes in solutions of chemotactic peptides], cell motion usually seems erratic, but, interestingly, local portions of the leading lamella move out at constant speed with fingerlike shapes.) Recognizing this unusual characteristic of cell spreading in concert with other experimental clues, the physics of amoeboid motion can be reduced to an easily understood set of dynamical actions. In the development to follow, the focus is on steady propagation of fixed-shape lamella patterns, because understanding how these simple kinematics arise from chemical and physical complexity will expose the underlying microscopic processes responsible for amoeboid movement. Two limiting cases of cell–substrate interaction (i.e. "strong" and "weak" adhesion) are examined to demonstrate the coupling of microscopic actin polymerization and network contraction to cell locomotion. In the context of these limiting cases, prominent features from recent experimental studies of mechanical contraction forces in phagocytes during engulfment of yeast particles (Evans, E., A. Leung, and D. Zhelev, submitted for publication) and actin network dynamics in locomoting fishscale keratocytes (12) are discussed to show the relation of experimental parameters to constitutive properties of actin assembly–contraction–disassembly processes. Even though grossly simplified, the comparison brings out crucial questions about the nature of microscopic physical–chemical actions.

Address correspondence to Dr. E. A. Evans, Department of Academic Pathology, University of British Columbia, 2211 Westbrook Mall, Vancouver, BC V6T 1W5, Canada.

## GENERAL CONSIDERATIONS

In view of the rapid movement of amoeboid cells (especially at mammalian body temperatures), the astonishing observation is that phagocytic cells appear to be enormously viscous when passive (13, 14). In the passive state, deformation response of the whole cell is liquidlike but exhibits an "apparent" viscosity $10^5$ times that of water! So, the obvious question is how can such lethargic bodies move so rapidly when activated? The answer seems to be that cells advance by rapid addition polymerization of actin at the lead boundary of the spreading


0006-3495/93/04/1306/17 $2.00

lamella (12, 15). Because the plasma membrane is easily pushed forward by cytosolic pressure, little mechanical energy is required to advance the lamella boundary; mainly, chemical energy is needed to fuel the actin polymerization process. Locomotion of the cell is produced by contraction of the actin network simultaneous with release of the rear portion of the cell from the substrate. The cell is pulled forward by network contraction through lamella-substrate traction. Here, some mechanical energy must be dissipated due to the contractile movement of the network relative to the cytosol and the hydrodynamic drag on cell body from translation in the aqueous environment; again, the magnitude can be small. Thus, nature has developed an optimal mechanism for cell motion that circumvents major dissipation of mechanical energy associated with whole cell deformation. On the other hand, when cells need to pass through small restrictions, there is sufficient contractility in the actin network to overcome the large transient resistance to the extreme deformation.

Even though the behavior in locomotion is clear (i.e., rapid spreading of the lamella and forward displacement of the cell), little is known about the physical coordination of network assembly, disassembly, and cell contraction. The basic physics for multiphase–multicomponent flow and chemical polymerization–depolymerization reactions is conventional science, and its application to cell motility has been described thoroughly in the past (7). However, the equations that express this general physics lead to extremely complex behavior that is further confounded by the nontrivial feature of moving boundaries. Fortunately, there are strong clues to the important dynamics in cell spreading that allow simplification of the physics. The most striking and frequent observation is linear growth, where local portions of lamellae and pseudopodia advance and retract uniformly over time (at constant velocity). Such behavior is characteristic of processes that are far from equilibrium (in the regime of mass action for chemical reactions) (16, 17). Consistent with linear growth, recent studies (12, 15) have shown that lamella spread by addition of material (actin), principally at the advancing boundary. The combined evidence indicates that the complexity of amoeboid motion can be reduced in the following ways. First, the microscopic dynamics (chemical–mass action and diffusion kinetics) for rapid polymerization of actin are localized to a narrow region along the advancing boundary. Second, cell contraction and translation are governed by slow macroscopic flow and disassembly of the network throughout the lamella coordinated with adhesion to and release from the substrate. Thus, the situation reduces to separate dynamical processes in two contiguous regions (see schematic Fig. 1). Evolution (shape versus time) of the lamella involves dynamical coupling between physical fields pinned to the lead boundary and homogenous fields distributed throughout the actin network (17).

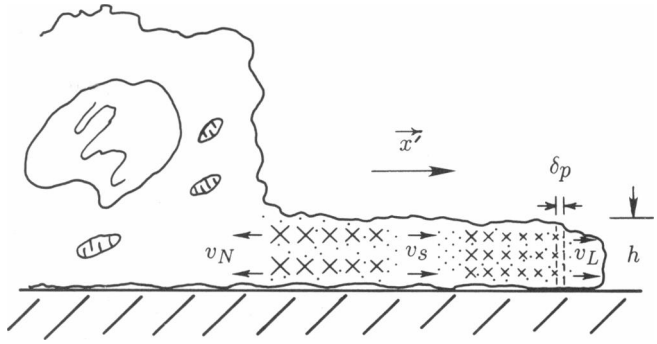


FIGURE 1 Schematic of the growth of a lamella projection from a cell body. Simplification of the physics leads to a description based on separate dynamical processes in two contiguous regions: first, rapid polymerization of actin in a microscopic layer $\delta_p$ along the advancing boundary, and second, slow macroscopic flow and disassembly of a contractile network embedded in the cytosol fluid throughout the lamella.

The kinematics of spreading and cell locomotion seem obvious in cases of constant velocity, *but,* the signals that turn on and/or off each phase remain subtle aspects. As will be shown later, the distinct feature of cell response is abrupt start–stop sequences with steady motion in between. The observation implies that the signals must be mediated by small molecules that rapidly diffuse through the cell. As such, the signal processes appear to take place over time scales much shorter than those for network assembly, contraction, and cell translation. Based on this observation, it is assumed that the dynamics of amoeboid motion decouple from the processes of stimulation. With the caveat of this assumption and the benefit of other observational clues, parsimonius physical models are readily developed for amoeboid spreading and contraction that exhibit the unusual kinematics of steady lamella growth.

## CELL SPREADING AND GROWTH OF LAMELLAE: THEORETICAL CONSIDERATIONS

Active cell spreading is the universal process by which cells form adhesive contacts with other cells and artificial substrates (Fig. 2). "Cells stick where they crawl!" This behavior is distinct from spontaneous wettinglike adhesion of liquid drops to surfaces that is driven by long range van der Waals and other attractive colloidal forces. (Although colloidal forces are ever present, they are so weak mainly because of steric separation between cell membranes and electrostatic repulsion that the attraction is not sufficient to overcome mechanical stiffness of the cell interface in order to produce large contacts.) As cells spread, surface receptors adhere to the substrate near the advancing boundary of lamella, are then translated rearward relative to the cell by motive contraction (apparently coupled to the cytoplasmic–actin network), and finally detach from the substrate at some rear loca-

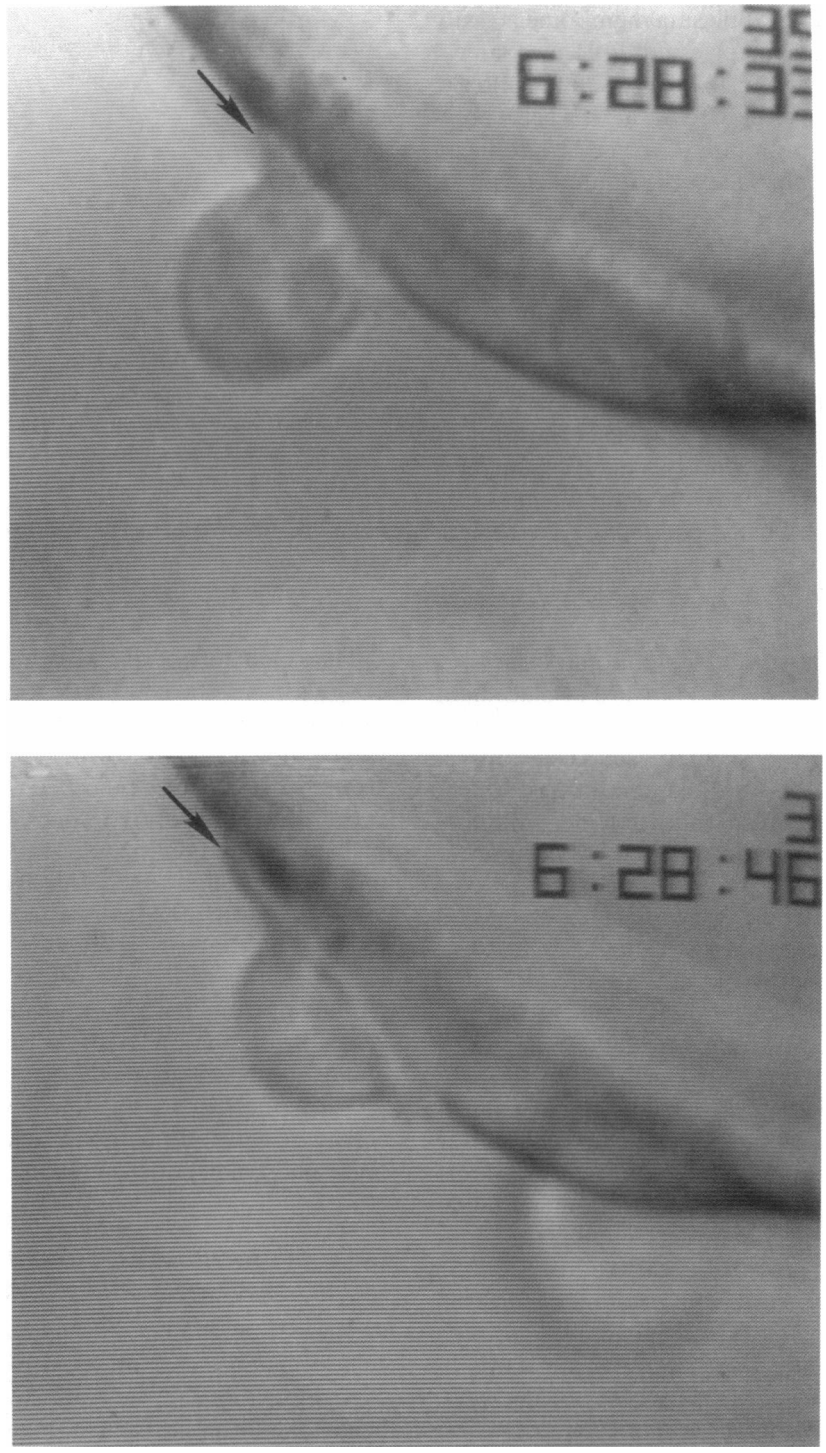


FIGURE 2 Videomicrographs of a granulocyte spreading on an endothelial cell surface demonstrate steady boundary advance with little or no motion of the lamella material. The arrows point to the lead edge of the lamella.

tion near the cell body. Throughout the retrograde motion, the lipid bilayer (plasma membrane) envelope advances forward (18) with the lamella contour (presumably by unwrinkling and flow outward from the cell body). A major subtlety in this process is that the receptors must eventually dissociate from the actin network near the cell body (perhaps facilitated by disassembly of the network) and then be transported (by diffusion or convection) back to the advancing boundary where they can again be coupled to the network. This aspect of motility alone is complicated and not understood at present. Analysis of experimental evidence (19) indicates that passive diffusion superposed on forward flow of the lipid bilayer can provide sufficient transport. The subsequent

reattachment of receptors to the actin network remains a mystery. The intricacies of cell adhesion–release will be neglected to focus on the dynamics of the lamella motion.

## Plasma membrane and cytosol kinematics

In lamella motion, the actin network core is the source of motive force. However, the processes of network assembly–contraction–disassembly live inside a plasma membrane envelope filled with cytosol fluid. Most likely, release of the plasma membrane from the network at the advancing boundary is necessary to enable polymerization. If so, then cytoplasmic turgor pressure would act to push the bilayer ahead of the network. This probably accounts for the ruffling and blebbing often observed along the perimeter of locomoting cells. Also, optically thin regions adjacent to the boundary are frequently observed with phase contrast microscopy. Conversely, polymerization is probably suppressed sterically when the membrane contacts the network. Because the bilayer is very fluid, the bilayer should not significantly impede actin network dynamics in the lamella unless restrained by contour stiffness. (Note that in the absence of fusion by lipid vesicles from cytoplasmic sources, plasma bilayer must be recruited from surface wrinkles and folds over the cell body. To increase lamella area, bilayer tension, scaled by the characteristic radius of curvature for the contour roughness, would have to the exceed cortical deformation stresses to smooth the contour.) Most important in lamella dynamics, the plasma membrane envelope establishes an impenetrable boundary to the flow of cytosol. Since the membrane remains close to the membrane interface, the cytosol advances at nearly the same speed as the rate of network growth which eliminates convected transport of actin monomers to the interface.

## Network kinematics

In phagocytes, advancing regions of lamella contours move forward rapidly with uniform rates of ~0.1–0.4 $\mu$m/s, but as evidenced qualitatively by the lack of movement of "lumplike" markers during granulocyte spreading (cf. Fig. 2), the interior networks remain nearly stationary. Even more convincing, elegant studies of fish-scale keratocytes have demonstrated directly the rearward motion of a local element of actin network relative to the moving cell shape (12). Hence, network material must be rapidly added (grown) by actin polymerization along the lamella boundary. Furthermore, network contraction and the boundary polymerization process must be steady in time local to the tip of the lamella to advance at constant speed. Away from the tip, changes in the boundary growth rate give rise to evolution of the lamella pattern over time. As yet, the detailed kinematics of the network velocity field along lamella contours are

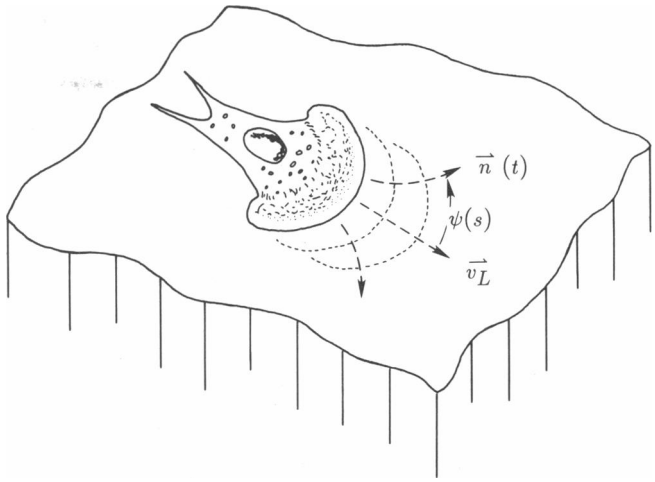


FIGURE 3 Schematic illustration of steady advance of fingerlike patterns, where the velocity normal to the boundary at any location $s$ along the contour is constant over time and leads to curved trajectories for the normal $\vec{n}(t)$ as shown. Although the lamella seems to be pushed forward, the pattern advances by mass addition to the network along the boundary where the kinematics of growth are governed by specific velocity conditions (Eq. 1 in the text).

not documented well enough to provide explicit definition of the polymerization process. However, local regions of lamella patterns appear frequently to advance with a steady fingerlike shape. (Note that for fixed-shape patterns, the angular orientation $\psi$ at each location $s$ along the contour of the boundary must remain constant over time as illustrated in Fig. 3.) In other words, the pattern seems to extend as if the lamella region is rigid and mass is only added at the rear junction with the cell body. However, steady pattern advance also can be produced by polymerization of a flowing network along its boundary. The kinematics of boundary growth must satisfy a specific velocity condition, i.e.,

$$v_p = -\vec{v}_N \cdot \vec{n}, \tag{1}$$

where $\vec{v}_N$ is the velocity of the preformed network relative to the fixed boundary shape, $\vec{n}$ is a unit vector normal to the contour, and $v_p$ is the polymerization-growth velocity given by the rate of mass addition $J_p$ (divided by local network concentration $\rho_N$) per unit area along the boundary. Because of the fixed shape pattern, it is convenient to examine fields in the coordinate system that translates steadily in time (at velocity $\vec{v}_L$). (Note that in the substrate [stationary] reference frame, network velocity $\vec{v}'_N$ is equal to $\vec{v}_N + \vec{v}_L$; the kinematics of growth are given by,

$$v_p = v_L \cos\psi - (\vec{v}'_N \cdot \vec{n}),$$

since $\vec{v}_L \cdot \vec{n} = v_L \cos\psi$.) In general, advance of fingerlike patterns with variable curvature will involve a continuous decrease in polymerization velocity along the contour away from the tip of the pattern. As such, growth,

coupled to the network velocity field, will be nonuniform; the polymerization velocity $v_p(s)$ will vary along the contour. Since steady pattern motion appears to be a prominent feature of amoeboid motion, the central question is: what constitutive laws for boundary polymerization, network contraction, and disassembly are consistent with this type of lamella advance and steady cell motion?

## Boundary polymerization and diffusional limitations

In boundary polymerization, chemical action is assumed to occur on a microscopic scale $\delta_p$ (local to the network interface) much smaller than the macroscopic dimensions of the network (cf. Fig. 1). Hence, the process is coupled to the local concentrations (number/volume) of actin monomer in the cytosol and network actin at the interface ($\rho_M$, $\rho_N$, respectively). Furthermore, the polymerization process must be far from equilibrium to be consistent with the steady growth of the lamella boundary. Therefore, the interfacial reaction can be represented by a local rate constant $k_M$ for conversion of actin monomers to network filaments, and the flux of material $J_p$ added to the interface is given by,

$$J_p = (\delta_p k_M)\rho_M = \rho_N \cdot v_p, \tag{2}$$

which defines the polymerization velocity $v_p$. The local rate constant $k_M$ depends on network concentration at the interface and perhaps other molecular constituents (e.g., actin binding proteins) in the polymerization process as well.

Since actin monomers are distributed throughout the cytosol, there can be nonlocal kinetic restrictions on the rate of network assembly because of diffusion from distant regions in the cell to the advancing boundary. Hence, monomer diffusion could slow the rate of advance. The rate of chemical polymerization at the boundary equals the diffusive flux of monomer through the cytosol to the boundary; the conservation relation is approximated by,

$$J_D \approx D(\rho_M^\infty - \rho_M)/\delta_D, \tag{3}$$

where $D$ is the diffusivity of monomeric actin in the lamella network, $\rho_M^\infty$ is the monomer concentration far from the boundary, and $\delta_D$ is the effective thickness of the diffusion boundary layer near the interface. As shown previously (17), the local balance (Eqs. 2 and 3) exposes the relation between growth and diffusive kinetics at a position on the boundary, i.e.,

$$\delta_D \approx D'(1 - v_p/\hat{v}_p)/v_p. \tag{4}$$

The boundary layer thickness $\delta_D$ is coupled directly to the polymerization velocity (where $D' = D\rho_M^\infty/\rho_N$ and $\hat{v}_p = \delta_p k_M \rho_M^\infty/\rho_N$). Obviously, high diffusivity leads to thin boundary layers; the network advances close to the maximum polymerization velocity $\sim \hat{v}_p$. On the other hand, low diffusivities lead to thick boundary layers (which expand over time); network growth is slowed progressively by diffusion limitations. The dynamic features expected for local growth regulated by diffusion are embodied in evolution properties of the local monomer depletion field $\Theta$ that is the cumulated depreciation of monomer concentration $\rho_M$ relative to reference concentration $\rho_M^\infty$ far from the boundary (17), i.e.,

$$\Theta \equiv \int_0^\infty [\rho_M^\infty - \rho_M(\xi)]\, d\xi \equiv \delta_D(\rho_M^\infty - \rho_M). \tag{5}$$

The depletion field $\Theta$ defines the thickness $\delta_D$ of the diffusion layer and is coupled directly to the local growth rate $v_p$ through Eqs. 2 and 3. The dynamic change of the depletion field predicts the slowing of the local growth rate as monomer diffusion becomes restrictive. Conservation of sources and/or sinks for the depletion field includes several contributions (17), but the major source for monomer depletion is the polymerization reaction itself. As such, the local velocity of polymerization should diminish with time according to (see Appendix 1),

$$\left[1 - \left(\frac{v_p}{\hat{v}_p^2}\right)\right]\frac{dv_p}{dt} \approx -\left(\frac{\rho_N}{\rho_M^\infty}\right)^2 \frac{v_p^3}{D}, \tag{6}$$

when limited by monomer diffusion. Clearly, growth at short times is unretarded by monomer diffusion and proceeds at the maximum polymerization velocity $\hat{v}_p$, but at long times, growth crosses over to diffusion-limited rates, i.e.,

$$v_p \sim \sqrt{D/t}.$$

Thus, the length $L(t)$ of a projection should eventually increase as $L \sim \sqrt{D \cdot t}$ that is not steady growth. The obvious conclusion is that diffusivity of actin monomer through the porous network must satisfy,

$$D > L^2/\Delta t_s,$$

over the period $\Delta t_s \sim L/v_L$ characteristic of the spreading process. Since $L \leq 10$ $\mu$m and $v_L \sim 0.1$ $\mu$m/s, the diffusivity must exceed 1 $\mu m^2/s$ ($10^{-8}$ $cm^2/s$). Although not well studied, measurements of diffusivity of G-actin in cells (20) are consistent with this requirement. Therefore, the velocity normal to the advancing boundary of lamellae is expected to closely approach the intrinsic polymerization velocity determined by the microscopic assembly of the F-actin network (represented by the rate constant $k_M$). The kinetics of actin polymerization at network interfaces are not known, but as we will see, specific conditions for boundary polymerization must be satisfied to achieve fingerlike pattern motion.

High magnification images of cortical networks in active cells (21) show that the polymerization process produces a random network along the boundary of the la-

mella. Hence, persistently disordered actin filaments must be grown in the cytosolic space adjacent to the network independent of local direction of advance. The likely scenario is that relatively short (disordered) F-actin filaments are rapidly polymerized in this space and cross-linked (e.g., by actin binding proteins) to the network interface. In addition, there could be continued growth of the preformed network filaments as well. To be consistent with experimental evidence that growth occurs locally to the boundary, most of the actively growing barbed ends of filaments would have to be blocked after leaving the interfacial region (toward the interior of the lamella). Since network filaments grow mainly in the vicinity of the interface, the growth can be represented by a boundary nucleation process coupled to the local network concentration $\rho_N$ at the boundary, e.g.,

$$k_M \approx \mathring{k}_M(\rho_N/\mathring{\rho}_N)^q, \quad (7)$$

where $\mathring{k}_M$ is the reaction rate at some reference network concentration $\mathring{\rho}_N$ and q is a phenomenological exponent that characterizes the order of the boundary nucleation process. As such, the polymerization velocity is governed by the following relation:

$$v_p \approx \mathring{v}_p(\rho_N/\mathring{\rho}_N)^{q-1}, \quad (8)$$

where $\mathring{v}_p$ is the polymerization velocity at the network reference concentration. The constitutive law (Eq. 8) embodies the microscopic chemical nature of the polymerization mechanism when unrestricted by monomer diffusion. A general feature is immediately apparent: if the exponent $q = 1$, then mass is added to the network in linear proportion to the network concentration along the boundary and the polymerization velocity $v_p$ would have to be constant. For this polymerization law, boundary contours would tend to advance without gradients in curvature and not exhibit fingerlike patterns. But if $q \neq 1$, then the polymerization velocity depends on the network concentration along the boundary. As such, the direction of growth or advance would coincide with an orientation given by the network concentration gradient and would exhibit pointed patterns (e.g., $q > 1$, the network concentration would be highest at the tip, and $q < 1$, the network concentration would be lowest at the tip). Intuitively, $q > 1$ is expected for a nucleation process; however, is this type of polymerization law consistent with cell motion and network biochemistry?

## Network disassembly

To produce steady cell translation, global conservation of network material is essential; this includes network polymerization, disassembly, and depolymerization processes. Two generic types of network disassembly processes in the lamella can be envisioned: bulk (homogeneous) and rear boundary (heterogeneous). In the first case, network is continuously disassembled after formation by relatively slow reactions. But in the second case, the network is disassembled rapidly at the rear boundary of the lamella. A mixture of both processes of network disassembly could exist. A possible clue to the behavior is indicated by biochemical properties of F-actin in vitro. Assuming that the free monomer concentration is relatively high, actin depolymerization will be very slow from the unblocked-pointed ends of filaments, much slower than polymerization (12, 22). Hence, rapid polymerization of network material along the boundary would be counterbalanced most easily by a homogeneous process of network disassembly throughout the lamella body. (It should be noted that disassembly of the network may proceed at a rate even faster than the rate of filament depolymerization. Breakup of the network occurs when topological connections are disrupted [e.g., arrangement of cross-links, defects, and entanglements].) For homogeneous disassembly, network concentration would decrease from the tip of the lamella toward the cell body. To be consistent with this concentration gradient, the boundary nucleation process for polymerization would have to be characterized by an exponent $q > 1$ (i.e., second order), that is, more dense network regions would grow faster along the boundary than less dense regions. There is clear evidence for homogeneous disassembly in experiments on fishscale keratocytes (12). The results support the intuition that the polymerization velocity along the boundary is an increasing function of local network concentration. To complete the conservation loop, some heterogeneous (rear boundary) disassembly may be needed, or, equivalently, the rear boundary may be thickened greatly to provide a boundary plenum for final depolymerization. In any case, given the boundary polymerization law (Eq. 8), the flow properties and disassembly of the network will determine the evolution of the lamella pattern.

## Network dynamics

Networks (consistent with the label) represent condensed phases where dynamics are governed by equations of motion for collective (mechanical) behavior. Because network segments are kinetically restricted by cross-links and entanglements, nonlocal effects due to diffusion of network segments are most likely negligible on the time scale of network motion. The result is that the dynamics of fingerlike amoeboid motion reduce conceptually to mechanical flow of the lamella network and cytoplasm with evolution of the boundary shape governed by the polymerization growth law (Eq. 8) and kinematic requirements (Eq. 1). Even though nonlocal features associated with diffusion have been eliminated, the situation remains complicated because the lamella material is a mixture of network and cytosol with complex rheological properties. The simplest approach is to treat the lamella material as two continuous phases living in the same space. Thus, mixture fields (e.g., concentration, velocity, stress) are superpositions of individual fields for the separate phases in proportion to their vol-

ume fractions (7). Furthermore, since 99% or so of the lamella is cytosol liquid, only variations in the small volume fraction or concentration of the network phase need be considered; the cytosol can be treated as an incompressible liquid that fills all space. Hence, the major emphasis is on movement of the network through the cytosol fluid.

Instead of describing the general equations of motion for the network and cytosol in three dimensions, the development is specialized here to cell lamellae (similar lines of reasoning can be followed for pseudopod-shape projections as well). Small scale irregularities (graininess) and motional variations are averaged through the cross-section of the lamella to leave dynamic fields (e.g., stress, velocity, concentration, and so on) and material properties in a form that embodies the mean transport of the material (17). The coarse-grained fields describe the motion in the plane of the substrate where concentration $\rho$, velocity $\vec{\mathbf{v}}$, and stress $\vec{\vec{\sigma}}$ fields are defined by,

$$\rho \equiv \frac{1}{h}\int \rho'(x_3)\,dx_3 \quad \vec{\mathbf{v}} \equiv \frac{1}{h}\int \vec{\mathbf{v}}'(x_3)\,dx_3$$

$$\vec{\vec{\sigma}} \equiv \frac{1}{h}\int \vec{\vec{\sigma}}'(x_3)\,dx_3, \tag{9}$$

and $h$ is the local lamella thickness. (Velocity and stress fields are vector $\vec{\mathbf{v}}$ and tensor $\vec{\vec{\sigma}}$ quantities where the arrows denote components corresponding to the two-dimensional coordinates ($\vec{\mathbf{x}}$) of the lamella pattern.) Clearly, there are separate concentration ($\rho_S$, $\rho_N$), velocity ($\vec{\mathbf{v}}_S$, $\vec{\mathbf{v}}_N$), and stress fields ($\vec{\vec{\sigma}}_S$, $\vec{\vec{\sigma}}_N$) for cytosol and network phases. As complementary ingredients, constitutive relations between stress and deformation (or rate of deformation) fields are required for the cytosol and network phases. To obtain expressions for mass and momentum (force) conservation, several factors guide the formulation and dictate boundary conditions. (*a*) Most of the lamella space is filled with incompressible fluid: the cytosol. Thus, because the plasma membrane envelope remains close to the network interface, the cytosol moves uniformly with the boundary of the lamella. (*b*) Since network topology is random, the macroscopic velocity fields ($\vec{\mathbf{v}}_S$, $\vec{\mathbf{v}}_N$) represent averages over microscopically disordered flows. Conceptually, then, viscous dissipation is reduced to a volume average of microscopic drag forces produced by motion of network segments relative to the cytosol. (*c*) Because the cytosol and plasma membrane envelope move with comparable velocity, drag of receptors through the plasma membrane (as the result of network attachments) contributes a retarding force that is also essentially proportional to the velocity difference between cytosol and network phases. (This is a crude approximation since the plasma membrane velocity can differ from the cytosol velocity interior to the lamella even though they coincide at the boundary. In addition, the relative velocity between membrane and cytosol depends on the distribution of contour roughness over the lamella.) (*d*) The traction of the cell on the substrate is created by interactions between cell surface receptors and the substrate; this traction is driven by network contraction through transmembrane connections. Recognizing these features, equations of motion for the lamella material are expressed as follows.

Mass conservation (continuity) of the cytosol is given by,

$$\bar{\nabla}\cdot(h\vec{\mathbf{v}}_S) + \frac{\partial h}{\partial t} = 0, \tag{10}$$

where $\bar{\nabla}$ is the two-dimensional gradient operator ($\partial/\partial x_1$, $\partial/\partial x_2$) in the plane of the lamella. Since cytosol moves uniformly with the boundary contour, the relative velocity is zero along the boundary (established by the proximity of an impermeable membrane envelope). (For fixed thickness and in the absence of circulating secondary flow, the cytosol velocity would be zero throughout the lamella in the coordinate system that moves with boundary). Mass conservation for the network is most conveniently expressed in terms of changes in network volume fraction $\phi_N = \nu_M\rho_N$, i.e.,

$$\bar{\nabla}\cdot(h\phi_N\vec{\mathbf{v}}_N) + \frac{\partial(h\phi_N)}{\partial t} = -\phi_N h/t_N, \tag{11}$$

where $1/t_N$ is the phenomenological rate of homogeneous network disassembly and $\nu_M$ is the molecular volume of a monomeric segment of the network. Equations for conservation of mass couple to equations for conservation of momentum (force balances) to fully describe motion.

Momentum conservation in a continuum is given by the sum of gradients (technically divergences) in material stress fields and locally applied forces. Stresses in each phase act in proportion to the volume fraction occupied by the phase. The volume fraction of cytosol is approximately one and cytosol stress is represented by a hydrostatic pressure field $P_S$. Dissipation in the cytosol fluid is dominated by interphase drag. To first order, interphase drag is assumed to be proportional to network concentration and the relative network–cytosol velocity, i.e.,

$$C_D\phi_N h(\vec{\mathbf{v}}_N - \vec{\mathbf{v}}_S),$$

where $C_D$ is the phenomenological drag coefficient (force/velocity/volume). Thus, momentum conservation in the cytosol fluid is given by,

$$-\bar{\nabla}(P_S h) + C_D\phi_N h(\vec{\mathbf{v}}_N - \vec{\mathbf{v}}_S) = 0. \tag{12}$$

(The viscous resistance to movement of receptors through the plasma membrane can be included in the approximation for interphase drag force but the coefficient $\bar{C}_D$ is scaled by the lamella thickness [e.g., $C'_D = C_D + \bar{C}_D/h$, where $\bar{C}_D$ = force/velocity/area].) In the

network phase, stresses may not be isotropic. A stress tensor or matrix is required to define local forces on an element of network material along independent directions. For a lamella projection, stresses include a component $\sigma_{N_\perp}$ perpendicular to the lamella that together with cytosol pressure must balance any external pressure applied to the upper surface of the lamella, i.e.,

$$-P_S + \phi_N \sigma_{N_\perp} \approx 0 \tag{13}$$

The other components are lateral stresses $\vec{\vec{\sigma}}_N$ represented by two principal stress components $\sigma_{N_1}$ and $\sigma_{N_2}$ in the plane of the lamella pattern. As will be shown next, gradients in network stresses (scaled by volume fraction $\phi_N$) are produced by interphase drag and cell-substrate traction.

A major contribution to network stress gradients is cell-substrate traction, but the mechanism is not universal. Dynamic properties of cell-substrate traction are completely unknown at present so some type of model must be introduced. The general scenario is that the lamella either sticks strongly to the substrate (which arrests network movement) or weakly interacts with the substrate (which allows the network to freely contract and to transport the cell body). Phenomenologically, extremes of traction can be represented by another viscous drag relation, $\bar{C}_T \phi_N (\vec{v}_N + \vec{v}_L)$, where the coefficient $\bar{C}_T$ (force/velocity/area) is conceived to be extremely large ($\sim\infty$) in the regime of strong substrate adhesion but modest in the regime of weak receptor interaction with the substrate. (The velocity $(\vec{v}_N + \vec{v}_L)$ is the velocity of the network observed in the substrate reference frame.) In this viscous relation for traction, it is assumed that the motive receptors are expressed in proportion to local network fraction $\phi_N$; obviously other dependencies are possible. Biochemical actions of receptor insertion, substrate bonding and/or release, and extraction are major processes in the traction mechanism and play significant roles in the coordination of spreading, contraction, and locomotion. But these actions are unknown at present and can only be treated phenomenologically.

Receptor–substrate traction is very important since it propels the cell over the surface. Including traction and interphase drag, gradients in lateral network stresses are given by,

$$\bar{\nabla} \cdot [\phi_N \vec{\vec{\sigma}}_N h] = C_D \phi_N h (\vec{v}_N - \vec{v}_S) + \bar{C}_T \phi_N (\vec{v}_N + \vec{v}_L). \tag{14}$$

Because of the stress condition on the upper surface (Eq. 13), the balance of lateral forces in the network can be combined with the cytosol pressure gradient (Eq. 12) to produce a useful-alternative form,

$$\bar{\nabla} \cdot [\phi_N (\vec{\vec{\sigma}}_N - \sigma_{N_\perp} \vec{\vec{I}}) h] \approx \bar{C}_T \phi_N (\vec{v}_N + \vec{v}_L), \tag{15}$$

where $\vec{\vec{I}}$ is the identity tensor. The equations of motion reduce to a set of network relations (Eqs. 11 and 15). These two equations are solved subject to appropriate boundary conditions and self consistent with the cytosol flow. Coupling to cytosol flow is through the thickness field $h(\vec{x})$; cytosol mass conservation (Eq. 10) and momentum conservation,

$$\bar{\nabla}(\phi_N \sigma_{N_\perp} h) \approx C_D \phi_N h (\vec{v}_N - \vec{v}_S),$$

yield the cytosol velocity field subject to the velocity boundary condition $\vec{v}_s \cdot \vec{n} \approx 0$ (in the moving pattern frame) and pressure boundary condition to be discussed next.

Spatial variations of network stresses are changes relative to appropriate boundary conditions along the network interface. The boundary conditions for stresses depend on the physical interaction between the plasma membrane and network at the lead edge. For example, if the plasma membrane (subject to a tension $\tau_m$ local to the interface) is detached from the network, then the stresses must satisfy,

$$\begin{aligned} \phi_N \sigma_{N_\perp} &\approx P_S \approx \tau_m / h \\ \vec{n} \cdot \vec{\vec{\sigma}}_N &\approx 0. \end{aligned} \tag{16}$$

On the other hand, stresses are specified by,

$$\begin{aligned} \phi_N (\vec{n} \cdot \vec{\vec{\sigma}}_N \cdot \vec{n}) - P_S &\approx \Delta P_N - \tau_m / h \\ \vec{n} \cdot \vec{\vec{\sigma}}_N \cdot \vec{t} &\approx \partial \tau_m / \partial s, \end{aligned} \tag{17}$$

if the membrane is bonded to the leading edge of the network. The first condition expresses the balance of hydrostatic pressure in the cytosol against the Laplace pressure created by membrane tension at the lead edge. However, if the network is bonded to the network interface (second condition), then the polymerization reaction would have to produce a mechanical pressure $\Delta P_N$ on the order of the Laplace pressure to push the plasma membrane outward (8).

Interior to the lamella, the local traction force is driven by gradients (Eq. 15) in the product of network density and deviatoric stress $(\vec{\vec{\sigma}}_N - \sigma_{N_\perp} \vec{\vec{I}})$, which is the combined stress for the network/cytosol mixture. When the lamella adheres strongly to the substrate, the network is held stationary; the speed of pattern advance is governed solely by the polymerization velocity at the boundary. By comparison, when network contraction is opposed weakly by the substrate, the mixture stress will be nearly constant because external drag forces are very small, especially at speeds observed for amoeboid movement. As such, strong forces of chemical contraction would be dissipated by internal processes within the network. The mixture stress would vary inversely with network density to keep the product constant. The velocity of cell translation is governed by the balance of net traction against the small drag force $\vec{F}_{CB}$ on the cell body produced by motion through the external aqueous environment,

$$\bar{C}_T \int\int \phi_N (\vec{v}_N + \vec{v}_L) \, d^2x = \vec{\vec{F}}_{CB}. \tag{18}$$

Because the network slides relative to the substrate, the cell body and lamella may translate at speeds less than the polymerization velocity.

## Network rheology

The final ingredient in the dynamics of motion is the rheological behavior of the network (i.e., the constitutive relation between stress and flow). Studies of in vitro rheology for actin networks show that stress can be a very complicated function of deformation and rate of deformation (23). Much less is known about the in situ rheology of cell networks. Phenomenologically (7, 17), network stress $\vec{\sigma}_N$ can be represented by the superposition of passive $\vec{\sigma}_N^p$ and active $\vec{\sigma}_N^c$ components, i.e., $\vec{\sigma}_N = \vec{\sigma}_N^p + \vec{\sigma}_N^c$. Passive stresses are coupled to deformation and rate of deformation by elastic ($K_N$, $\mu_N$) and viscous ($\kappa_N$, $\eta_N$) coefficients, e.g., lateral stresses in an ideal viscoelastic material would be given by,

$$\vec{\sigma}_N^p \approx (K_N\nu + \kappa_N\dot{\nu})\vec{I} + 2\mu_N\vec{\epsilon}_S + 2\eta_N\vec{V}_S, \qquad (19)$$

where $\nu$, $\dot{\nu}$ are the local network dilation and rate of dilation, and $\vec{\epsilon}_s$, $\vec{V}_s$ are the local network shear strain and rate of shear tensors. Active stresses are chemically generated and may not be isotropic fields because of orientational order among network filaments. (For minimal ordering of the network, the active stress would be approximated by $\vec{\sigma}_N^c = \sigma_N^c\vec{I}$.) Examining network rheology in the context of limiting cases for substrate traction provides insight into the general consequences of network rheology.

In the *strong* adhesion regime, deformation and rate of deformation fields are constrained except for thickness changes:

$$\nu \approx \Delta h/h_0 \qquad \vec{\epsilon}_S, \vec{V}_S \approx 0.$$
$$\dot{\nu} \approx \frac{1}{h}\frac{\partial h}{\partial t}$$

Lateral network stresses are purely contractile and opposed rigidly by substrate attachment. Only the principal stress $\sigma_{N_\perp}$ in the thickness direction is unrestrained. Thus, to maintain constant thickness, the contractile stress in the thickness direction would either have to be balanced largely by elastic or steric compressional forces approximated by,

$$K_{N_\perp}(\Delta h/h_o) + \sigma_{N_\perp}^c = P_S/\phi_N \approx 0,$$

or be small because of orientational ordering of the network parallel to the substrate. (The hydrostatic pressure $P_s$ in the cytosol fluid is probably not large since it is on the order of the turgor pressure in the cell body. Furthermore, since contractile stresses in the network reach 0.01 Atm, the osmotic pressure created by proteins in solution also can be neglected unless the protein concentrations exceed $10^{-3}$ M.)

In the *weak* adhesion regime, lateral network stresses remain small because of weak traction, and network contractility drives network condensation. In a freely contracting state, dynamic–viscous stresses should exceed elastic stresses so that the network will condense at a rate $\dot{\nu}$ on the order of the ratio of contractile stress to viscosity, i.e.,

$$\dot{\nu} = \vec{\nabla}\cdot\vec{v}_N + \frac{\partial(\ln h)}{\partial t} \approx -\sigma_N^c/\kappa_N \equiv -1/t_c.$$

This ratio defines a characteristic relaxation time $t_c$ for free contraction. Because of the free boundary condition at the upper surface of the lamella, the stress field would have to be anisotropic to preserve a nearly uniform thickness as the network condenses. Anisotropy could result from orientational ordering of filaments parallel to the substrate. In addition, dynamic contraction could lead to unstable roughening of the surface unless smoothed by other mechanisms. Clearly, prediction of the lamella thickness is an important requirement for physical models, but this must be undertaken in careful detail. Such analyses necessitate precise definition of network constitutive properties and major numerical computation. However, as a first approximation, the essential physical concepts can be illustrated under the assumption that lamella thickness is constant and that contraction acts only parallel to the plane of motion. Applying this abstraction to the limits of strong and weak substrate adhesion, network rheological properties can be represented crudely by two relaxation times ($t_c$, $t_c'$): a rate of stress increase $1/t_c'$ when the network is constrained by adhesion and a rate of condensation $1/t_c$ when the network is unrestrained.

## UNIFORM PATTERN ADVANCE AND NETWORK CONTRACTION FOR STRONG AND WEAK ADHESION: COMPARISON OF SIMPLE MODELS TO CELL BEHAVIOR

In this section, very simple analyses will be introduced to expose the relation between experimental data and basic physical mechanisms in the regimes of strong and weak substrate adhesion. Two specific examples of amoeboid activity will be used to demonstrate application of the theoretical development to diverse cell behavior. Because of the idealized approach, comparison between the simple analyses and experimental data is first order, leaving out many details of amoeboid motion. However, important features of the cell dynamics correlate with the approximations and indicate major aspects to be investigated in future experiments. Details of the impact of strong and weak adhesion limits on the equations of motion for networks in lamellae are given in Appendix 2 along with the approach for more refined analysis.

### Strong substrate adhesion

As discussed, strong substrate adhesion acts to restrain network motion; the network appears not to move in the substrate-based reference frame (cf. Fig. 2). The contractile stress builds up at an intrinsic rate $1/t_c'$ governed by chemical processes that progressively tighten the net-

work (e.g., myosin molecular "motors" or gelation mechanisms). The lamella contour advances at a speed $v_L$ established by the rate of polymerization along the network boundary. For fingerlike patterns, the local kinematic requirement for steady pattern motion becomes simply,

$$v_p \approx v_L \cdot \cos\psi$$
$$v_N \approx -v_L \qquad v_S \approx 0, \tag{20}$$

where the unidirectional network and cytosol velocities are defined in the coordinate system that moves with the pattern. If the pattern is curved, then the polymerization velocity must decrease along the pattern contour. In the abstraction of constant lamella thickness (see Appendix 2), a single equation dominates the dynamics: the conservation of network mass approximated by,

$$v_L \frac{d}{dx}(\phi_N) = -\phi_N / t_N$$
$$v_p \frac{ds}{dx} = v_L \frac{dw}{dx},$$

where both the width $w$ of the lamella and network concentration field depend only on the axial distance $z$ from the lamella tip ($z = L - x$) driven by the rate $1/t_N$ of network disassembly. This equation gives a simple result that the network volume fraction attenuates with distance rearward from the lamella tip,

$$\phi_N / \dot{\phi}_N \approx e^{-z/t_N v_L}.$$

Network concentration is coupled to pattern advance by the boundary polymerization process and the kinematic requirement in Eq. 20, i.e.,

$$\cos\psi \approx e^{-(q-1)z/t_N v_L},$$

which establishes the shape of the pattern. The result predicts that the curvature $1/R_L$ at the lamella tip is governed by the ratio of network disassembly rate to maximum polymerization velocity at the tip (here given by the speed of advance $v_L$),

$$1/R_L \approx (q-1)/t_N v_L.$$

For steady growth of a fingerlike pattern, actin polymerization along the network boundary would have to be a second-order process ($q > 1$) coupled to homogeneous disassembly of the network. Refinement of the analysis to allow network slip relative to the substrate is described in Appendix 2.

Recent biophysical tests of phagocyte contractility during pathogen engulfment provide data for lamella spreading and network contraction in the regime of strong substrate adhesion (Evans, E., A. Leung, and D. Zhelev, submitted for publication). These experiments demonstrate both linear growth (constant spreading velocity) and steady increase of contractile stress with time. Briefly, the experiment (illustrated in Fig. 4) is designed to observe engulfment of a yeast particle and simultaneously measure contractile force in a stimulated phagocyte (a blood granulocyte). Contractile forces are evaluated in an isometric condition where the cell body length is held constant by a suction inside a pipet. Drawn in initially by small pressures of $\sim 10^2$ dyn/cm$^2$, the length of the passive cell reaches $\sim 25$ $\mu$m. Maneuvered by another pipet, a zymosan (yeast) particle is then touched to the exposed end of the granulocyte that, after a brief period, spontaneously spreads over the yeast particle. As required, the suction pressure is adjusted to keep the length of the stimulated cell constant inside the pipet. Examination of the first sequence of spreading and contraction yields consistent serial behavior; i.e., the lamella spreads and engulfs the yeast at constant velocity, but no contractile force is detectable in the cell body until spreading has stopped (or nearly stopped). Then, contractile force increases steadily with time without spreading on the yeast particle. Typical results for the initial sequence of engulfment and cell body contraction are plotted in Fig. 5; the measurements (over time) include cell body length $L_c$, lamella advance $L_e$ over the yeast, and pipet suction $P$. The data clearly demonstrate steady lamella growth and abrupt start/stop kinetics of the spreading and contraction phases. The most impressive observation is that the contractile stress (imaged by the suction pressure) rises from low values of $10^2$ dyn/cm$^2$ (approximately the initial turgor pressure in the cell body) to maximum levels of $2\text{–}4 \times 10^4$ dyn/cm$^2$. Using the pipet cross-section of $\sim 10^{-7}$ cm$^2$, contractile force in a single cell is found to reach $10^{-3}$ dyn or more.

In relation to the simple analysis for strong substrate adhesion, the rate of lamella advance over the yeast yields the polymerization velocity with values of $0.1\text{–}0.2 \times 10^{-4}$ cm/s; also, network stress in the cell body rises steadily at rates of 200–400 dyn/cm$^2$/s. Measurements of contractile force provide important in situ data that can be compared with models proposed for force generation in actin networks. The myosin molecular "motor" is the most popular model where myosin molecules ratchet actin filaments past one another in the network (24, 25). When constrained, forces on the order of $10^{-7}$ dyn can be produced by these molecular motors (25, 26). Forces of cell contraction in these isometric tests indicate that $>10^4$ motors would be necessary to fulfill the task. Equivalently, the myosin concentration in a granulocyte would have to exceed $10^{-7}$ M. This concentration is well within the range of data for myosin content in granulocytes (28). Likewise, gelation/solation of actin networks is expected to be an important aspect of cell motility (27). Actin experiments in vitro (28) show that the duration of contraction is directly correlated with ratios of actin/myosin and actin/filamin. The values of 60–70 s measured for phagocytes stimulated by yeast particles correspond to actin/myosin ratios < 10:1 and actin/filamin ratios > 200:1 in

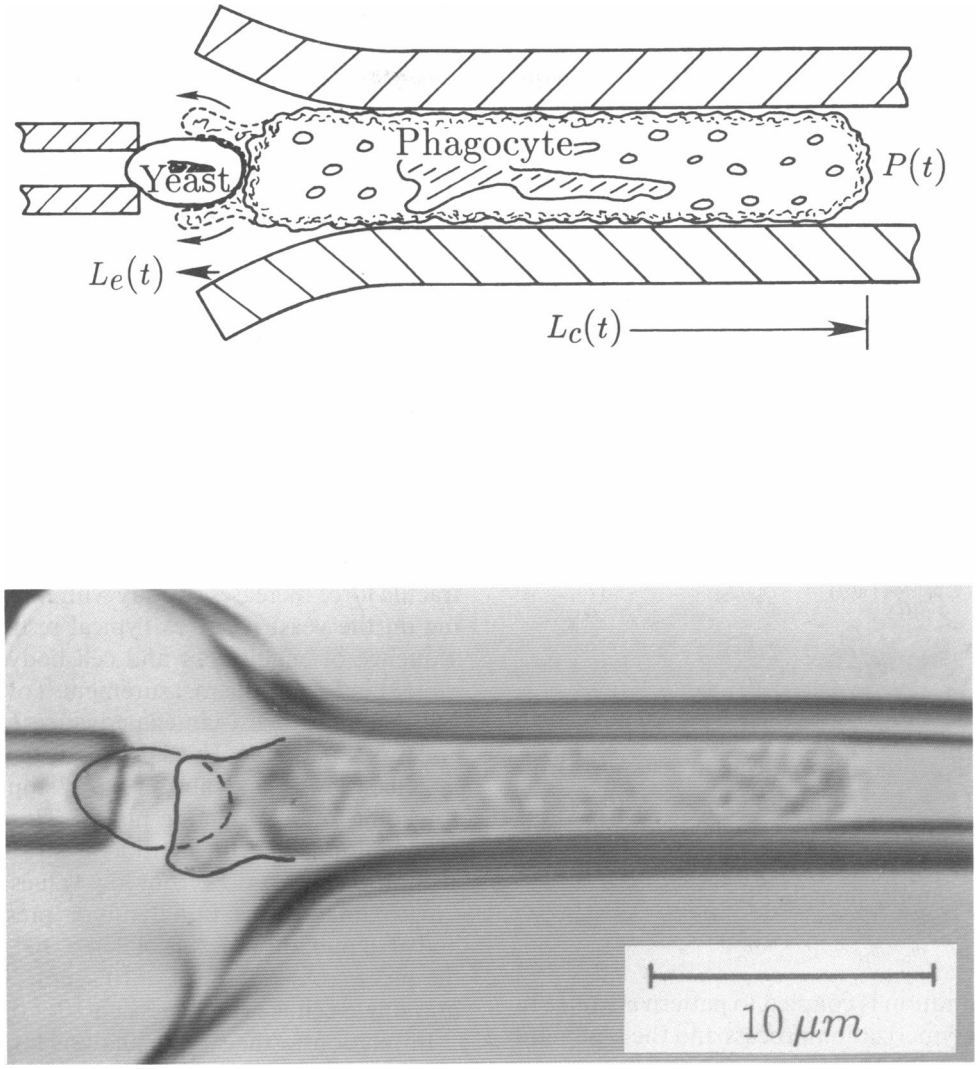


FIGURE 4 Illustration of the method used to study the sequence of lamella advance (over a yeast particle) and contraction force in a phagocyte held at fixed length by pipet suction.

vitro. This evidence indicates that actin networks in phagocytes are loose weakly cross-linked structures. The steady rate of increase in contractile stress with the cell body length held constant may reflect steady tightening of loose network arrangements ("pulling out the slack").

## Weak substrate adhesion

The important feature of the weak adhesion regime is that network contraction is little impeded by substrate traction. The net traction balances the hydrodynamic resistance to cell body translation and determines the speed of locomotion. Depending on the spatial distribution of traction forces and network slip relative to the substrate, the translation speed can be significantly less than the polymerization velocity at the lead edge of lamella. In the limit that traction and network-cytosol drag forces are much weaker than network contractile stresses, a simple analysis serves to illustrate the salient features of pattern shape, network velocity, and cell motion. In the limit of free contraction (see Appendix 2), the network can be assumed to condense uniformly at an intrinsic rate $1/t_c$ (again with constant lamella thickness). Thus, the network velocity is simply proportional to radial distance $r$ from a central position in the pattern as shown by the circular divergence of the velocity field,

$$\frac{1}{r}\frac{d}{dr}(rv_N) \approx -1/t_c,$$

i.e., $v_N \sim -r/2t_c$. Seeking solutions that are stationary (over time) in the radial coordinate, conservation of network mass again dominates the dynamics,

$$\frac{1}{r}\frac{d}{dr}(r\phi_N v_N) \approx -\phi_N/t_N. \qquad (21)$$

Solution of this equation shows that network concentration can either increase or decrease with radial position

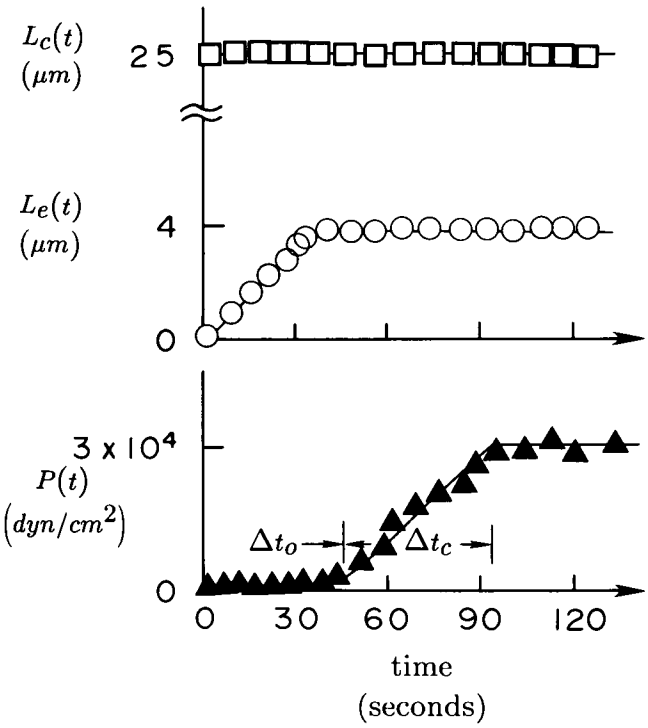


FIGURE 5 Serial sequence of spreading and cell body contraction observed consistently in tests of yeast engulfment by blood granulocytes. Cell body length $L_c$, lamella advance $L_e$ over the yeast particle, and the pipet suction P required to hold $L_c$ constant were measured simultaneously as shown (data taken from a single cell test at 23°C).

depending on the ratio of rate of free contraction ($1/t_c$) to rate of disassembly ($1/t_N$) in the network, i.e.,

$$\phi_N \approx \phi_N(R)[r/R]^{(2t_c/t_N-2)}.$$

To keep network concentration finite near the central position, the rate of disassembly would have to be at least twice the rate of contraction. With this simple model of free-uniform contraction, the kinematic requirement for boundary advance (Eq. 1) and the constitutive law for boundary polymerization velocity (Eq. 8) are easily satisfied by a circular contour where the radius $R$ is specified by,

$$R = 2t_c \cdot v_p, \tag{22}$$

given the relation for $v_p = f[\rho_N(R)]$ since $v_p = -v_N$ at the boundary. Thus, the size $R$ of the model cell pattern is set by the rate of contraction $1/t_c$ and the polymerization velocity $v_p$. In the moving frame of the pattern, the network retracts rapidly from the stationary boundary and slows down progressively toward the central position. The circular contour is fixed in time, so what is the velocity of pattern translation?

To determine the rate of pattern advance, traction forces and hydrodynamic resistance to cell body movement through the environment have to be balanced. This depends on the model used to represent traction. The viscous traction model in Eq. 18 is a naive choice predicated on the assumption that receptors are driven by network contraction to slip over the substrate, thereby creating a drag force. Furthermore, it is assumed that motive receptors are expressed at the surface in proportion to network concentration. The model is purely speculative and only introduced to demonstrate the limit of weak substrate adhesion. Given the caveat that all or part of this model may be wrong, it remains a useful metaphor to demonstrate the distinction between cell translation velocity and lamella growth. As shown by the simple free contraction analysis, significant gradients in network velocity are expected for the situation of weak substrate adhesion. In the context of viscous traction, network velocity gradients will lead to differential forces on the substrate. In fact, traction at the rear of the lamella opposes advance, whereas the dominant traction near the front promotes forward motion. This is obvious from the integral in Eq. 18,

$$v_L = -\langle v_N \rangle + F_{CB} \Big/ \bar{C}_T \iint \phi_N \, d^2x, \tag{23}$$

where,

$$\langle v_N \rangle = \iint \phi_N (\vec{v}_N \cdot \vec{i}) \, d^2x \Big/ \iint \phi_N \, d^2x$$

$$\vec{v}_L \equiv v_L \vec{i}.$$

When the simple free contraction result is introduced, i.e.,

$$\langle v_N \rangle = -v_p \iint \tilde{r}^{(2t_c/t_N)} \cos\psi \cdot d\tilde{r} \cdot d\psi \Big/ \iint \tilde{r}^{(2t_c/t_N-1)} \, d\tilde{r} \cdot d\psi$$

$$\tilde{r} \equiv r/R.$$

Eq. 23 relates the observed speed $v_L$ of pattern advance to the concentration average of the network velocity $\langle v_N \rangle$ and the external fluid drag force. Since velocities of 0.1–0.4 $\mu$m/s for cell locomotion are slow, the hydrodynamic resistance to cell translation through the environment is very small. Hence, as a first approximation, the external fluid drag force $F_{CB}$ can be neglected, i.e., $F_{CB} \sim 0$. As such, the density average of the network velocity $\langle v_N \rangle$ essentially specifies the cell translation velocity $v_L$. By simple calculation, the translation speed is always less than the velocity of polymerization at the pattern tip as shown in Fig. 6 for shapes defined by circular segments (size specified by the angular arc $\hat{\psi}$). Clearly, when traction (network concentration) is large near the boundary ($t_c/t_N \gg 1$), the translation speed approaches the polymerization velocity for narrow segments ($\hat{\psi} < \pi/6$). Except for the special case of a half circular segment ($\hat{\psi} = \pi/2$), a residual flux of network material exists at the rear boundary of the pattern that is not dealt with in the simple analysis. (The residual flux would create a pileup

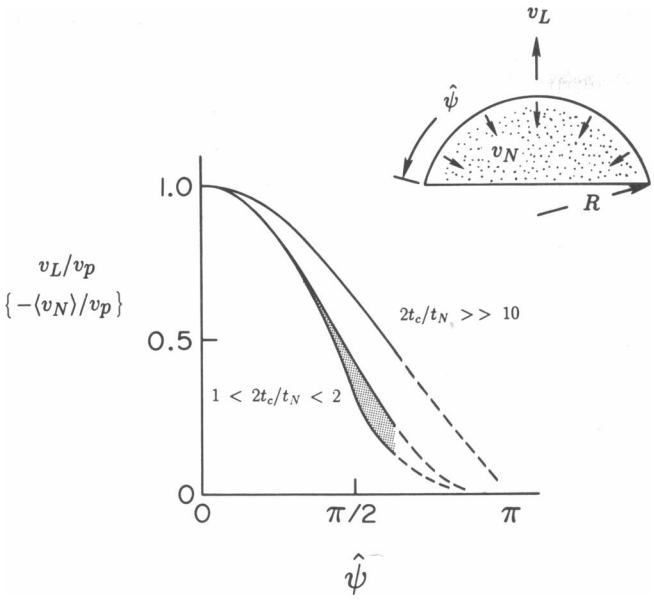


FIGURE 6 Prediction of the velocity $v_L$ for translation of a circular-segment pattern (defined by radius $R$ and angular arc $\hat{\psi}$) driven by uniform network contraction. Motive receptors attached to the network are assumed to produce viscous traction (in direct proportion to network density) by sliding over the substrate. The translation velocity is always less than the velocity $v_p$ for polymerization of network along the circular boundary and depends on the ratio of rate of network disassembly to rate of network contraction ($t_c/t_N$). The shaded area represents situations where the rate of disassembly does not greatly exceed the rate of contraction ($1 < t_c/t_N < 2$). For the upper curve, the rate of contraction is much smaller than the rate of disassembly. The intrinsic polymerization velocity $v_p$ and rate of contraction $1/t_c$ govern the size $R = t_c v_p$ of the pattern.

of material and thickening of the cell along the back boundary. The thickened border could provide a plenum of sufficient size to complete network disassembly.)

Although the circular idealization of a freely contracting network is crude, it brings out subtle features of amoeboid dynamics that can be overlooked easily by an observer. First, fields that are independent of time in the moving frame can vary strongly in time for an observer because of moving gradients; the time rate of change measured by an observer is,

$$\frac{\partial}{\partial t}(\cdots) = -v_L(\vec{\mathbf{i}} \cdot \bar{\nabla})(\cdots).$$

Second, because of network velocity gradients (contraction) and slip relative to the substrate, the cell body will translate at speeds slower than the polymerization velocity. Thus, some region of the network will appear stationary to an observer, i.e., where $\vec{\mathbf{v}}_N + \vec{\mathbf{v}}_L = 0$ or where $\langle v_N \rangle = v_N$ in the viscous traction model. Furthermore, on either side of this location, network material will seem to move in opposite directions. Last, the rate of network "turnover" measured by an observer is the difference between the actual rate of disassembly and the rate of contraction ($1/t_N - 1/t_c$).

The subtle features just described are clearly evident in studies of actin network dynamics in locomoting fishscale keratocytes (12). Even though fishscale keratocytes are different cells from a different species, they move with steady velocities of order 0.1–0.5 $\mu$m/s comparable with the human granulocyte shown in Fig. 2. The astonishing observation is that the cell pattern (half-moon in shape $\hat{\psi} \approx \pi/2$) remains essentially constant as the cell translates steadily over the substrate. (This has stimulated concepts of tank-tread motion, but careful measurements [12] have effectively ruled out such kinematics.) As noted in reference 12, locomoting keratocytes do not appear to make close-focal contacts with the substrate, which implies weak adhesion for steadily advancing cells. In these studies, the impressive accomplishment was to expose motion and turnover of the actin network within the lamella. By microinjection of actin conjugated with a special "caged" fluorphore, the authors were able to photoactivate a small region of the actin network to produce a fluorescent patch. Because of the low bleach quality of the fluorphore, the fluorescence emission persisted for long periods of time so that network dynamics could be measured. Based on their observations, the authors concluded that ". . . actin microfilaments in the lamella remain approximately fixed relative to the substrate . . . regardless of speed. The rate of turnover of actin subunits . . . is remarkably rapid." The data presented in their article (cf. Fig. 4i and 4j in reference 12) support their conclusions with one subtle exception: the actin network was not immobile. The fluorescent patterns showed definite spatial contraction in addition to progressive attenuation of intensity over time. In particular, the sides of the fluorescent images converge toward a stationary position, i.e., network ahead of the fixed position moved rearward (relative to the substrate) but network behind this position actually moved forward. Contraction is especially prominent in the data for a bipolar cell ($\hat{\psi} \approx \pi$) that was held fixed by lamellae pulling in opposite directions at each end (cf. Fig. 4j in reference 12). Likewise, observations of distance versus time for transport of concanavalin A coated beads attached to receptors on keratocytes show similar gradients of velocity (i.e., the beads slow down as they move rearward from the boundary; cf. Fig. 3 in reference 29).

The simple idealization of a freely contracting network provides a rationale for these observations as illustrated in Fig. 7. Fig. 7 *a* is a cartoon of the half-moon shape of a locomoting keratocyte with a patch of network fluorescence; the cell moves forward with a steady velocity $v_L$. Fig. 7 *b* illustrates the instantaneous velocities that would be detected by an observer for the semicircular model of the lamella network and cell; the sketch demonstrates both the velocity jump at the bound-

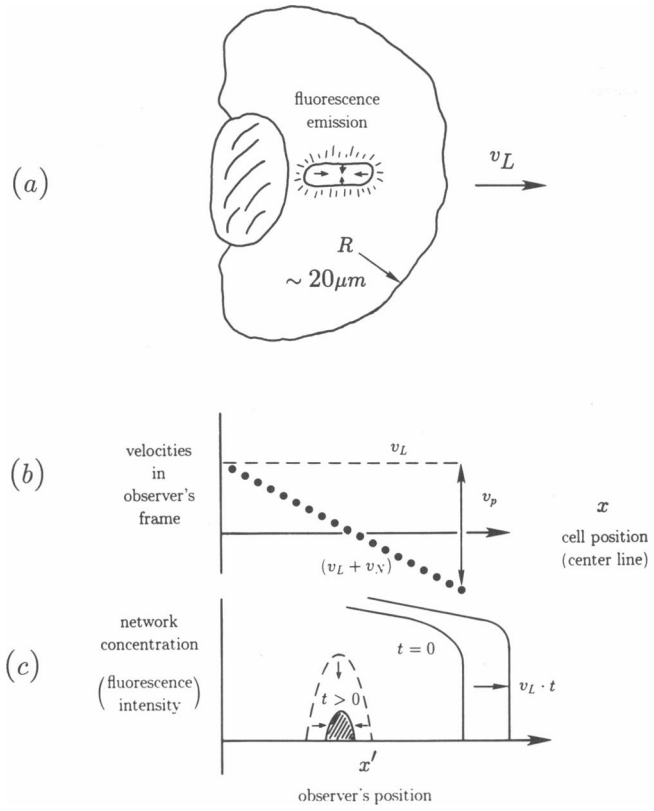


FIGURE 7 (*a*) Schematic of the region of emission from fluorescently-labeled network material along the center line in the lamella of a steadily advancing fish-scale keratocyte. The illustration portrays elegant experiments developed by Theariot and Mitchison (12). (*b*) Sketch of the network velocity field $v_N$ (in the cell-based frame) plus the speed $v_L$ of cell body translation over the substrate as predicted by simple radial contraction model with polymerization along the circular boundary. The velocity jump along the advancing boundary is produced by the polymerization velocity $v_p$. The location of the-zero-velocity crossing would appear stationary in the substrate-based frame. The cell coordinate $x$ (measured forward from the rear of the cell along the center line) is related to the observer position $x'$ (measured along the substrate) by $x' = x + v_L t$. (*c*) Schematic of the fluorescence pattern (–network concentration) that would be seen by an observer as the cell moves across the field of view. Although the fluorescence intensity (network concentration) appears to decrease with time for the observer, the network concentration is only a function of position in the cell pattern. Also, at first glance, the fluorescence image seems not to move but closer inspection shows that the image contracts towards the middle, which follows from the velocity characteristics illustrated in (*b*).

ary produced by polymerization and the zero velocity crossing determined by the ratio of translation velocity to polymerization velocity. Clearly, ahead and behind the crossing (which forms a line across the semicircular pattern), network converges toward the crossing with negative and positive velocities, respectively. Fig. 7 *c* illustrates the fluorescence intensity measured by an observer as the cell advances across the field of view (indicated by the boundary displacement $v_L t$). The fluorescence intensity both attenuates and narrows (driven by network contraction) over time but appears not to move! The rate of decrease in fluorescence intensity at the center of the pattern is governed by competition between network disassembly and network contraction, i.e., $1/t_N - 1/t_c$. In reference 12, the measurements of decrease in fluorescence intensity over time yielded apparent values of 23 s for network turnover. However, the rate of contraction deduced from narrowing of the fluorescent images over time appears even faster where $2t_c$ is on the order of 15 s. These values imply that the rate of network disassembly is probably much faster than the observed turnover rate (i.e., $t_N \sim 6$ s). Another prediction of the simple model is that the characteristic radius $R$ of the cell is given by the polymerization velocity $v_p$ along the circular boundary multiplied by twice the characteristic contraction time (i.e., $R \approx 2v_p t_c$). This implies that the polymerization velocity at the lead edge of a fishscale keratocyte is $\geq 1$ μm/s.

Recent experiments (30) have greatly extended the work reported in reference 12; here, interesting higher order dynamic effects have been examined for actin networks in locomoting fishscale keratocytes. These authors have nicely shown that the lamella advances by displacement normal to the boundary. Thus, the process of mass addition is local growth by interfacial polymerization (17) where kinematics are governed by Eq. 1. Network contraction toward the central nucleus is again evident in time-lapse images of fluorescence from network elements. In addition, there appears to be some retardation of network motion by substrate interactions that seems to be enhanced near the advancing boundary. Commensurate with the impedance to network contraction, radial ridges (spokelike thickenings) in the lamella pattern emanate from the cell nucleus; retardation causes the radial spokes to rotate toward the rear boundary of the cell. This type of organized roughening of thickness points to the sensitive stress boundary condition for the upper surface of the lamella (cf. Eq. 13) that may be only marginally stable at uniform thickness. Another eye-catching detail is that network material is not completely disassembled by the time it reaches the rear boundary of the lamella. Here, pileup of material is shown by thickening of the cell and deflection of network trajectories proximal to the rear boundary; thus, final network turnover probably occurs in this plenum.

The simple idealization sketched in Fig. 7 for the weak adhesion regime neglects any retardation of the network by interactions with the substrate. At the other extreme, network is completely immobilized by strong adhesion to the substrate. Clearly, the network dynamics in fishscale keratocytes fall somewhere in between these extremes. As such, the network velocity relative to the advancing boundary exhibits both a strong radial gradient and some angular (rearward) component (see Appendix 2 for the method of analysis). Because of the traction

effect, there could be a gradient in network concentration along the advancing boundary to produce a gradient in polymerization velocity and distortion of the circular contour. In addition to network density gradients, nonuniform network stress fields and variations in thickness become important so that dynamics are no longer governed simply by two-dimensional mass conservation at fixed thickness. Full analysis is obviously more complicated but manageable with sophisticated numerical computations. Network constitutive behavior remains the significant uncertainty. Even though full study of the higher order details of network dynamics is essential, the simple abstractions used here have both exposed important subtleties of network motion (overlooked by experimentalists) and boundary polymerization plus provided a direct connection between the observed kinematics of motion and the microscopic processes of network polymerization–contraction–disassembly.

## APPENDIX 1

Derivation of Eq. 6 in the text follows directly from the time rate of change of the monomer depletion field $\Theta$ local to the polymerization front, i.e.,

$$\frac{d\Theta}{dt} = \frac{d}{dt}\{\delta_D(\rho_M^\infty - \rho_M)\}, \tag{A1}$$

where both the thickness $\delta_D$ of the diffusion boundary layer and the concentration $\rho_M$ of monomers at the interface depend on time. By definition (Eq. 5), the depletion field cumulates the deviation in monomer content over the total volume (when scaled by the height and width of the lamella). Thus, if there are no sources for monomer in the volume (e.g., no network depolymerization), then the depletion field will increase with polymerization as monomers are converted to network, i.e.,

$$\frac{d\Theta}{dt} \approx J_p = \rho_N v_p. \tag{A2}$$

Both boundary layer thickness and monomer concentration at the interface are coupled to the polymerization velocity $v_p$. First, in the regime of mass action, far from chemical equilibrium, the polymerization velocity is simply proportional to monomer concentration at the interface as given by Eq. 2, i.e.,

$$v_p/\hat{v}_p = \rho_M/\rho_M^\infty. \tag{A3}$$

Second, the rate of polymerization at the interface is fed by the diffusion flux of monomers, i.e.,

$$\rho_N v_p \approx D(\rho_M^\infty - \rho_M)/\delta_D. \tag{A4}$$

Together, Eqs. A3 and A4 specify the depletion field $\Theta$ as a function of instantaneous polymerization velocity, i.e.,

$$\Theta \approx \frac{D(\rho_M^\infty)^2}{\rho_N}\left(\frac{1}{v_p} - \frac{2}{\hat{v}_p} + \frac{v_p}{\hat{v}_p^2}\right).$$

Hence, the time derivative of the depletion field governs the rate of change of polymerization velocity and lamella growth,

$$\frac{d\Theta}{dt} \approx \frac{D(\rho_M^\infty)^2}{\rho_N}\left(\frac{1}{\hat{v}_p^2} - \frac{1}{v_p^2}\right)\frac{dv_p}{dt}. \tag{A5}$$

Finally then, Eqs. A2 and A5 yield Eq. 6 in the text, i.e.,

$$\left[1 - \left(\frac{v_p}{\hat{v}_p}\right)^2\right]\frac{dv_p}{dt} \approx -\left(\frac{\rho_N}{\rho_M^\infty}\right)^2 \frac{v_p^3}{D},$$

or,

$$\left[1 - \left(\frac{v_p}{\hat{v}_p}\right)^2\right]\frac{dv_p}{dt} \sim -\frac{v_p^3}{D}. \tag{A6}$$

The evolution of the polymerization velocity with time is obviously of the form,

$$\left[1 - \left(\frac{v_p}{\hat{v}_p}\right)^2\right] + \left(\frac{v_p}{\hat{v}_p}\right)^2 \ln\left(\frac{v_p}{\hat{v}_p}\right)^2 \sim \frac{v_p^2 t}{D},$$

which implies that $v_p \sim \hat{v}_p$ when $t < D/\hat{v}_p^2$ and $v_p^2 \sim D/t$ at longer times. Since the length $L$ of the projection is essentially the integral of the growth velocity, the length will eventually approach,

$$L \sim \int v_p\, dt \to (D \cdot t)^{1/2}.$$

## APPENDIX 2

Equations of motion for the lamella network are given by Eqs. 11 and 15 in the text. Coupled to the network constitutive relations, these equations are solved subject to the appropriate boundary conditions for stress (Eq. 16 or 17) and velocity (Eqs. 1 and 8). Network flow is made compatible with cytosol flow through the thickness field $h(\vec{x})$. The general approach to solution is very complicated and requires major numerical computations. Even if this monumental task is accomplished, it is difficult to extract wide-ranging insights from a plethora of computational snapshots. Here, a minimal representation of network rheology will be invoked to demonstrate a method of solution and to expose important features of lamella dynamics in the limits of strong and weak adhesion to the substrate.

First of all, network stresses will be treated as predominantly planar (i.e., $|\vec{\sigma}_N| \gg |\sigma_{N_\perp}|$). This represents a network that is orientationally ordered parallel to the substrate and where the network-cytosol drag is small ($c_D \sim 0$). As such, the internal dynamics of the network dominate network rheology. For constant lamella thickness, the equations of motion reduce to

$$\vec{v}_N \cdot \vec{\nabla}(\ln \phi_N) \approx -1/t_N - \vec{\nabla} \cdot \vec{v}_N$$
$$\frac{1}{\phi_N}\vec{\nabla} \cdot (\phi_N \vec{\vec{\sigma}}_N) \approx \frac{\vec{C}_T}{h}(\vec{v}_N + \vec{v}_L). \tag{A7}$$

Thus, network traction on the substrate is driven by gradients in lateral stresses $\vec{\sigma}_N$.

By direct analogy to observations of myosin dynamics on single actin filaments (25), it will be assumed that the network is driven to contract parallel to the substrate by microscopic "motors," whose rates of displacement are limited by molecular dissipation. For filaments that are oriented randomly in the plane of the lamella, the continuum abstraction of the microscopic action is a superposition of lateral contraction stress $\sigma_c$ plus a dynamic impedance $\kappa(\vec{\nabla} \cdot \vec{v}_N)$ to contraction,

$$\vec{\vec{\sigma}}_N \approx [\kappa(\vec{\nabla} \cdot \vec{v}_N) + \sigma_c]\vec{\vec{I}}. \tag{A8}$$

Therefore, at small rates of contraction, network stress approaches the full strength of contraction. On the other hand, when the network contracts freely (no stress), the rate of contraction is limited to $-1/t_c =$

$-\sigma_c/\kappa$. For this type of constitutive behavior, the equations of motion (Eq. A7) for the network depend on a characteristic length $l_c = t_c \mathring{v}_p$ (where the polymerization velocity $\mathring{v}_p$ is the value at the lamella tip) and two dynamic ratios: i.e., one is the ratio $t_c/t_N$ for rate of network disassembly to rate of contraction and the other depends on the ratio of viscous traction to contractile stress,

$$\tilde{C}_T \equiv \left(\frac{C_T \mathring{v}_p}{\sigma_c}\right)\left(\frac{t_c \mathring{v}_p}{h}\right). \tag{A9}$$

Scaling velocities by $\mathring{v}_p$ and lengths by $l_c$,

$$\vec{\mathbf{u}} \equiv \vec{\mathbf{v}}_N/\mathring{v}_p, \quad \vec{\mathbf{u}}_L \equiv \vec{\mathbf{v}}_L/\mathring{v}_p = u_L \vec{\mathbf{i}}_z, \quad u_p \equiv v_p/\mathring{v}_p$$
$$\tilde{\mathbf{z}} \equiv \vec{\mathbf{x}}/l_c, \quad \tilde{\nabla}(\cdots) \equiv l_c \bar{\nabla}(\cdots),$$

the equations of motion are cast in a dimensionless (universal) form,

$$\vec{\mathbf{u}} \cdot \tilde{\nabla}(\ln \phi_N) \approx -t_c/t_N - \tilde{\nabla} \cdot \vec{\mathbf{u}}$$
$$\sigma \tilde{\nabla}(\ln \phi_N) + \tilde{\nabla}\sigma \approx \tilde{C}_T(\vec{\mathbf{u}} + \mathbf{u}_L \vec{\mathbf{i}}_z)$$
$$\sigma \equiv \tilde{\nabla} \cdot \vec{\mathbf{u}} + 1. \tag{A10}$$

The solutions for velocity and concentration fields must satisfy the velocity condition along the lead edge of the lamella given by,

$$u_p = -\vec{\mathbf{u}} \cdot \vec{\mathbf{n}} = (\phi_N/\dot{\phi}_N)^{q-1},$$

and an appropriate stress boundary condition.

With this minimal representation of network dynamics in the lamella, the limits of strong and weak adhesion to the substrate are explicitly characterized by,

$$\tilde{C}_T \gg 1 \Rightarrow \sigma \sim 1,$$

and

$$\tilde{C}_T \ll 1 \Rightarrow \sigma \sim 0,$$

respectively. The simple models discussed in the text are extremes where either $\tilde{C}_T \to \infty$ or $\tilde{C}_T \to 0$. For these limits, the equations of motion are simply,

$$\tilde{C}_T \to \infty \Rightarrow \vec{\mathbf{u}} + \vec{\mathbf{i}}_z = 0$$

$$\vec{\mathbf{i}}_z \cdot \tilde{\nabla}(\ln \phi_N) = t_c/t_N = \frac{d(\ln \phi_n)}{dz},$$

and

$$\tilde{C}_T \to 0 \Rightarrow \tilde{\nabla} \cdot \vec{\mathbf{u}} = -1$$

$$\vec{\mathbf{u}} = -\left(\frac{\tilde{r}}{2}\right)\vec{\mathbf{i}}_r, \quad \tilde{r} \equiv r/l_c, \quad \tilde{R} \equiv 2l_c$$

$$\vec{\mathbf{u}} \cdot \tilde{\nabla}(\ln \phi_N) = 1 - t_c/t_N = -\left(\frac{\tilde{r}}{2}\right)\frac{d(\ln \phi_N)}{d\tilde{r}}.$$

The next order of approximation can be built up from the solutions for these extremes through perturbations to the velocity $\delta\vec{\mathbf{u}}$ and concentration $\delta\phi_N$ fields, i.e.,

$$(\vec{\mathbf{u}} + \delta\vec{\mathbf{u}}) \cdot \tilde{\nabla}(\ln \phi_N) + \vec{\mathbf{u}} \cdot \tilde{\nabla}(\delta\phi_N) \approx -t_c/t_N - \tilde{\nabla} \cdot \vec{\mathbf{u}} - \tilde{\nabla} \cdot \delta\vec{\mathbf{u}}$$

$$(\sigma + \delta\sigma)\tilde{\nabla}(\ln \phi_N) + \sigma\tilde{\nabla}(\delta\phi_N) + \tilde{\nabla}(\sigma + \delta\sigma)$$
$$\approx \tilde{C}_T(\vec{\mathbf{u}} + u_L \vec{\mathbf{i}}_z + \delta\vec{\mathbf{u}})$$

$$\delta\sigma \equiv \tilde{\nabla} \cdot \delta\vec{\mathbf{u}}.$$

For strong substrate adhesion, ($\tilde{C}_T \gg 1$). The next level of approximation is found to be,

$$\delta\vec{\mathbf{u}} \approx (1 - u_L)\vec{\mathbf{i}}_z + \frac{1}{\tilde{C}_T}\left[\left(\frac{t_c}{t_N}\right)(\tilde{\nabla} \cdot \delta\vec{\mathbf{u}})\vec{\mathbf{i}}_z + \tilde{\nabla}(\delta\phi_N)\right]$$

$$(-\vec{\mathbf{i}}_z + \delta\vec{\mathbf{u}}) \cdot \left(\frac{t_c}{t_N}\right)\vec{\mathbf{i}}_z - \vec{\mathbf{i}}_z \cdot \tilde{\nabla}(\delta\phi_N) \approx -\left(\frac{t_c}{t_N}\right) - \tilde{\nabla} \cdot \delta\vec{\mathbf{u}},$$

This approximation is actually valid to order $(1/\tilde{C}_T^2)$. Since $|\tilde{\nabla}(\delta\phi_N)| \gg |\tilde{\nabla} \cdot \delta\vec{\mathbf{u}}|$, the concentration perturbation essentially obeys,

$$\tilde{\nabla}^2(\delta\phi_N) - \tilde{C}_T \frac{\partial(\delta\phi_N)}{\partial z} \approx \tilde{C}_T\left(\frac{t_c}{t_N}\right)(u_L - 1),$$

subject to boundary conditions at the tip of the lamella given by,

$$\delta\phi_N = 0 \quad \vec{\mathbf{i}}_z \cdot \delta\vec{\mathbf{u}} = 0$$

$$\frac{\partial(\delta\phi_N)}{\partial z} = \tilde{C}_T(u_L - 1) - (t_c/t_N)\tilde{\nabla} \cdot \delta\vec{\mathbf{u}}.$$

For weak substrate adhesion ($\tilde{C}_T \ll 1$), the approximate equations of motion become,

$$\frac{2(\delta\sigma)}{\tilde{r}}\left(\frac{t_c}{t_N} - 1\right)\vec{\mathbf{i}}_r + \tilde{\nabla}(\delta\sigma) \approx \tilde{C}_T\left[-\left(\frac{\tilde{r}}{2}\right)\vec{\mathbf{i}}_r + u_L \vec{\mathbf{i}}_z\right]$$

$$\left[-\left(\frac{\tilde{r}}{2}\right)\vec{\mathbf{i}}_r + \delta\vec{\mathbf{u}}\right] \cdot \left[\frac{2}{\tilde{r}}\left(\frac{t_c}{t_N} - 1\right)\vec{\mathbf{i}}_r\right] - \left(\frac{\tilde{r}}{2}\right)\vec{\mathbf{i}}_r \cdot \tilde{\nabla}(\delta\phi_N)$$
$$\approx \left(1 - \frac{t_c}{t_N}\right) - \tilde{\nabla} \cdot \delta\vec{\mathbf{u}}$$

The velocity perturbation is made up of both radial $\delta u_r$ and angular $\delta u_\psi$ components. The balance of network forces yields two separate equations,

$$\frac{2(\delta\sigma)}{\tilde{r}}\left(\frac{t_c}{t_N} - 1\right) + \frac{\partial(\delta\sigma)}{\partial\tilde{r}} \approx \tilde{C}_T\left[-\left(\frac{\tilde{r}}{2}\right) + u_L \cos\psi\right]$$

$$\frac{1}{\tilde{r}}\frac{\partial(\delta\sigma)}{\partial\psi} \approx -\tilde{C}_T(u_L \sin\psi),$$

which are coupled to the scalar conservation of mass,

$$\frac{2}{\tilde{r}}\left(\frac{t_c}{t_N} - 1\right)\delta u_r - \frac{\tilde{r}}{2}\frac{\partial(\delta\phi_N)}{\partial\tilde{r}} \approx -\frac{1}{\tilde{r}}\frac{\partial(\tilde{r}\delta u_r)}{\partial\tilde{r}} - \frac{1}{\tilde{r}}\frac{\partial(\delta u_\psi)}{\partial\psi}.$$

These equations are solved with the stress perturbation separated into two radial functions ($\delta\bar{\sigma}$, $\delta\sigma_z$) such that,

$$\delta\sigma \approx \delta\bar{\sigma} + \delta\sigma_z \cos\psi.$$

Likewise, the velocity perturbation is defined by,

$$\delta u_r \approx \delta u_z \cos\psi + \delta\bar{u}$$
$$\delta u_\psi \approx -\delta u_z \sin\psi,$$

where $\delta u_z$ and $\delta\bar{u}$ are also functions of radius related to the stress perturbation by,

$$\delta\bar{\sigma} = \frac{1}{\tilde{r}}\frac{d(\tilde{r}\delta\bar{u})}{d\tilde{r}}$$

$$\delta\sigma_z = \frac{d(\delta u_z)}{d\tilde{r}}.$$

The velocity component $\delta u_z$ is a rearward flow driven by traction and scales as $\tilde{C}_T u_L$. Finally, the density and velocity perturbations must

satisfy the velocity requirement (Eq. 1) along the lead edge of the lamella,

$$\left(\frac{\partial u_p}{\partial \phi_N}\right)\delta\phi_N \approx -\delta u_r,$$

given that $\delta u_r$ and $\delta\phi_N$ are zero at $\psi = 0$. Thus, for $\psi > 0$, the velocity condition along the lead edge will involve a slight departure from the unperturbed circular shape.

This work was supported by National Institutes of Health grants HL-45099 and HL-31579.

*Received for publication 10 July 1992 and in final form 10 December 1992.*

## REFERENCES

1. Southwick, F. S., and T. P. Stossel. 1983. Contractile proteins in leukocyte function. *Sem. Hematol.* 20:305–321.
2. Stossel, T. P. 1984. Contribution of actin to the structure of cytoplasmic matrix. *J. Cell Biol.* 99:15s–21s.
3. Stossel, T. P., J. H. Hartwig, H. L. Yin, and O. Stendahl. 1980. The motor of amoeboid leukocytes. *Biochem. Soc. Symp.* 45:51–63.
4. Valerius, N. H., O. Stendahl, J. H. Hartwig, and T. P. Stossel. 1981. Distribution of actin-binding protein and myosin in polymorphonuclear leukocytes during locomotion and phagocytosis. *Cell.* 24:195–202.
5. Hartwig, J. H., R. Neidermann, and S. E. Lind. 1985. Cortical actin structures and their relation to mammalian cell movements. *In* Subcellular Biochemistry. Vol. 11. D. B. Roodyne, editor. Plenum Press, New York. 1–49.
6. Odell, G. M. 1977. Amoeboid motions. *Lect. Appl. Math.* 16:191–220.
7. Dembo, M., and F. Harlow. 1986. Cell motion, contractile networks, and the physics of interpenetrating reactive flow. *Biophys. J.* 50:109–121.
8. Zhu, C., and R. Skalak. 1988. A continuum model of protrusion of pseudopod in leukocytes. *Biophys. J.* 54:1115–1138.
9. Oster, G. F., and A. S. Perelson. 1987. The physics of cell motility. *J. Cell Sci.* 8(Suppl.):35–54.
10. DiMilla, P. A., K. Barbee, and D. A. Lauffenburger. 1991. A mathematical model for the effects of adhesion and mechanics on cell migration. *Biophys. J.* 60:15–37.
11. Deleted in proof.
12. Theriot, J. A., and T. J. Mitchison. 1991. Actin microfilament dynamics in locomoting cells. *Nature (Lond.).* 352:126–131.
13. Valberg, P. A., and H. A. Feldman. 1987. Magnetic particle motions within living cells: measurement of cytoplasmic viscosity and motile activity. *Biophys. J.* 52:551–561.
14. Evans, E., and A. Yeung. 1989. Apparent viscosity and cortical tension of blood granulocytes determined by micropipet aspiration. *Biophys. J.* 56:151–160.
15. Mitchison, T., and M. Kirshner. 1988. Cytoskeletal dynamics of nerve growth. *Neuron.* 1:761–772; Forsher, P., and S. J. Smith. 1988. Actions of cytochalasins on the organization of actin filaments and microtubules in neuronal growth cone. *J. Cell Biol.* 107:1505–1516; Symons, M. H., and T. J. Mitchison. 1991. Control of actin polymerization in live and permeabilized fibroblasts. *J. Cell Biol.* 114:503–513.
16. Kessler, D. A., J. Koplik, and H. Levine. 1988. Pattern selection in fingered growth phenomena. *Adv. Phys.* 37:255–339.
17. Evans, E., and M. Dembo. 1990. Physical model for phagocyte motility: local growth of a contractile network from a passive body. *In* Biomechanics of Active Movement and Deformation of Cells. N. Akkas, editor. NATO ASI Series. Vol. H42. Springer-Verlag, Berlin. 185–214.
18. Lee, J., M. Gustafsson, K.-E. Magnusson, and K. Jacobson. 1990. The direction of membrane lipid flow in locomoting polymorphonuclear leukocytes. *Science (Wash. DC).* 247:1229–1233.
19. Ishihara, A., B. Holifield, and K. Jacobson. 1988. Analysis of lateral redistribution of a plasma membrane glycoprotein—monoclonal antibody complex which occurs during cell locomotion. *J. Cell Biol.* 106:329–343.
20. Jacobson, K., and J. Wojcieszyn. 1984. The translation mobility of substances within the cytoplasmic matrix. *Proc. Natl. Acad. Sci. USA.* 81:6747–6751.
21. Hartwig, J. H., and H. L. Yin. 1988. The organization and regulation of the macrophage actin skeleton. *Cell Motil. Cytoskeleton.* 10:117–125.
22. Pollard, T. D., and J. A. Cooper. 1986. Actin and actin-binding proteins: a critical evaluation of mechanisms and functions. *Annu. Rev. Biochem.* 55:987–1035.
23. Janmey, P. 1991. Mechanical properties of cytoskeletal polymers. *Curr. Opin. Cell Biol.* 2:4–11.
24. Kron, S. J., and J. A. Spudich. 1986. Fluorescent actin filaments move on myosin fixed to glass surface. *Proc. Natl. Acad. Sci. USA.* 83:6272–6276.
25. Ishijima, A., T. Doi, K. Sakurada, and T. Yanagida. 1991. Sub-piconewton force fluctuations of actomysin *in vitro*. *Nature (Lond.).* 352:301–306.
26. Huxley, A. F. 1957. Muscle structure and theories of contraction. *Prog. Biophys. Biophys. Chem.* 7:255–318.
27. Taylor, D. L., and M. Fechheimer. 1982. Cytoplasmic structure and contractility. The solation-contraction coupling hypothesis. *Phil. Trans. Soc. Lond. B Biol. Sci.* 299:185–197.
28. Janson, L. W., J. Kolega, and D. L. Taylor. 1991. Modulation of contraction by gelation/solation in a reconstituted motile model. *J. Cell Biol.* 114:1005–1015.
29. Kucik, D. F., S. C. Kuo, E. L. Elson, and M. P. Sheetz. 1991. Preferential attachment of membrane glycoproteins to the cytoskeleton at the leading edge of lamella. *J. Cell Biol.* 114:1029–1036.
30. Lee, J., A. Ishihara, J. A. Theriot, and K. Jacobson. 1993. Principles of locomotion for simple-shaped cells. *Nature (Lond.).* In press.